Scientific and Social Research, 2025, Volume 7, Issue 1
https://ojs.bbwpublisher.com/index.php/SSR
Online ISSN: 2981-9946
Print ISSN: 2661-4332

Efficient Photocatalytic Degradation of Tetracycline with Hydrothermally Synthesized Pure-Phase $BiFeO_3$

Lebing Liu*

Suzhou University of Science and Technology, Suzhou 215004, Jiangsu Province, China

***Corresponding author:** Lebing Liu, liulebing7989@163.com

Abstract: Tetracycline pollution poses an increasing global threat to both aquatic and terrestrial biodiversity due to its extensive use in aquaculture, livestock farming, and human disease prevention. In this study, pure-phase $BiFeO_3$ was synthesized using the hydrothermal method. Various characterization techniques, including X-ray diffraction (XRD), scanning electron microscopy (SEM), and X-ray photoelectron spectroscopy (XPS), were employed to analyze the material's crystal structure, surface morphology, and electron valence states. A 120-minute photocatalytic degradation experiment on tetracycline (TC) demonstrated that the pure-phase $BiFeO_3$ achieved a degradation efficiency of approximately 27%. The primary degradation mechanism was attributed to the generation of •OH (hydroxyl radicals) during the photocatalytic reaction, with h^+ (holes) playing a synergistic role. The energy band structure and photocatalytic mechanism of pure-phase $BiFeO_3$ were further analyzed using Ultraviolet-visible spectroscopy (UV-VIS-DRS). Cycling tests indicated that pure-phase $BiFeO_3$ maintained chemical stability, highlighting its potential for large-scale applications.

Keywords: Pure-phase BiFeO3; Tetracycline degradation; Photocatalytic efficiency; Mechanism

Online publication: January 23, 2025

1. Introduction

Tetracycline (TC), a widely used synthetic antibiotic, is commonly employed in treating various diseases in both humans and animals. While they effectively inhibit protein synthesis in bacteria, their widespread use has led to significant environmental pollution [1–2]. Among various treatment methods such as Fenton processes, ozonation, UV photolysis, and sonolysis, advanced oxidation processes (AOPs) have been developed to address the inefficiency of conventional methods in removing TC antibiotics from wastewater [3–4]. Among AOPs, photocatalysis stands out due to its strong redox ability, low cost, long durability, and resistance to adsorption saturation. These attributes make it a promising solution for scalable wastewater treatment aimed at degrading

micropollutants, and producing low toxic intermediates [5–6]. Commonly used photocatalysts like TiO_2 have limitations, including low efficiency under visible light and rapid recombination of photon-generated electron-hole pairs, which reduce their effectiveness in practical applications [7].

Bismuth ferrite ($BiFeO_3$, BFO) has emerged as a highly promising photocatalyst for the degradation of tetracycline (TC) due to its unique properties. Unlike TiO_2, which primarily responds to ultraviolet light due to its wider bandgap, $BiFeO_3$ exhibits a narrow bandgap (2.0–2.6 eV), enabling it to harness visible light and greatly enhancing solar light absorption efficiency. This makes $BiFeO_3$ particularly advantageous for real-world applications where visible light constitutes a significant portion of the solar spectrum. Additionally, the distortion of the lone-pair Bi 6s orbitals in these bismuth-based complex oxides facilitates the overlap between the O 2p and Bi 6s orbitals in the valence band, enhancing the migration of photon-induced charges and significantly improving photocatalytic efficiency. Numerous studies have demonstrated the visible light-driven photocatalytic activity of $BiFeO_3$ in the degradation of organic pollutants [8–9].

2. Experimental section

2.1. Preparation of pure-phase BiFeO3

To prepare pure-phase $BiFeO_3$, different samples were synthesized using the hydrothermal method: First, 5 mmol of $Bi(NO_3)_3 \cdot 5H_2O$ and 5 mmol of $Fe(NO_3)_3 \cdot 9H_2O$ (1:1 stoichiometric ratio) were added to the inner liner of a 25 ml hydrothermal reactor. Then, 18 ml of 8 mol/L KOH solution was added, and the mixture was stirred magnetically for 30 minutes. The reactor was sealed tightly and placed in an oven at 180°C for 6 hours, with a ramp-up time of 80 minutes and a cooling time of 800 minutes (heating rate of 2°C/min and cooling rate of 0.20°C/min). After the reaction, the product was filtered and washed three times with deionized water and anhydrous ethanol and then dried naturally. This material was named BFO-1. Similarly, 2.5 mmol of $Bi(NO_3)_3 \cdot 5H_2O$ and 2.5 mmol of $Fe(NO_3)_3 \cdot 9H_2O$ (1:1 stoichiometric ratio) were added to the inner liner of a 25 ml hydrothermal reactor. The same procedure was followed, with the addition of 18 ml of 8 mol/L KOH solution, magnetic stirring for 30 minutes, sealing, and heating in an oven at 180°C for 6 hours. The product was filtered, washed, and dried as previously described, resulting in the material named BFO-2. In another variation, 5 mmol of $Bi(NO_3)_3 \cdot 5H_2O$ and 5 mmol of $Fe(NO_3)_3 \cdot 9H_2O$ (1:1 stoichiometric ratio) were used with 18 ml of 6 mol/L KOH solution. The same hydrothermal procedure was followed, and the final product, after filtering, washing, and natural drying, was named BFO-3.

2.2. Characterization

X-ray diffraction (XRD) was performed with a Bruker D8 Advance diffractometer, utilizing Cu Kα radiation (λ = 1.5406 Å) to determine the crystal structure. The morphologies of the photocatalysts were analyzed using scanning electron microscopy (SEM) with a JEOL-7800F ZEISS and high-angle annular dark-field scanning transmission electron microscopy (HAADF-STEM), along with X-ray energy dispersive spectroscopy (EDX) for elemental mapping using a JEOL-2100F. The surface composition and oxidation states of the samples were analyzed via X-ray photoelectron spectroscopy (XPS) with an ESCALAB 250XI instrument. UV–vis diffuse reflectance spectra were recorded in the range of 200–800 nm using a Hitachi UH4150 spectrophotometer.

2.3. Photocatalytic performance test

The photocatalytic reaction was conducted in a quartz vessel using a 300 W xenon lamp equipped with a 420 nm

cut-off filter to block UV light. The vertical distance between the lamp and the reaction vessel was maintained at 15 cm. To prevent thermal effects on the results, the quartz vessel was cooled by circulating water, ensuring the temperature remained at room temperature. During the photocatalytic process, 50 mL of a tetracycline solution with a concentration of 20 mg/L was introduced into the quartz vessel, followed by the addition of 20 mg of catalyst powder. Continuous magnetic stirring was applied to ensure uniform dispersion of the catalyst in the solution. Before initiating the reaction, the mixture was stirred in the dark for 30 minutes to achieve adsorption-desorption equilibrium between the catalyst and the tetracycline molecules. Subsequently, 3 mL samples were collected at 30-minute intervals under light irradiation. The catalyst powder was separated from the solution using high-speed centrifugation. The absorption spectra of the collected samples were recorded using a UV-2450 spectrophotometer over the wavelength range of 200-800 nm. The degradation rate was calculated using the following formulas [23].

$$\text{Degradation}(\%) = (C_0 - C_t / C_0) \times 100\% = (A_0 - A_t / A_0) \times 100\% \quad (1)$$

$$\ln(C_t / C_0) = -kt \quad (2)$$

Where C_0 denotes the initial concentration of tetracycline, C_t represents the real-time concentration, A_0 indicates the initial absorbance, A_t is the absorbance at the time of measurement, and *K* stands for the rate constant.

3. Results and discussion

3.1. XRD analysis

As is shown in **Figure 1**, the XRD pattern of sample BFO-1 matches well with the standard data from JCPDS Card No.86-1518, confirming a rhombohedral perovskite structure belonging to the R3c space group [10–11]. All diffraction peaks of BFO-1 correspond to the standard card, with peaks at 2θ = 22.41°, 31.75°, 32.07°, 38.95°, 39.48°, 45.75°, 51.31°, and 51.74° corresponding to the (012), (104), (110), (006), (202), (024), (116), and (122) crystal planes, respectively. No secondary or heterogeneous phase diffraction peaks were observed [10, 12].

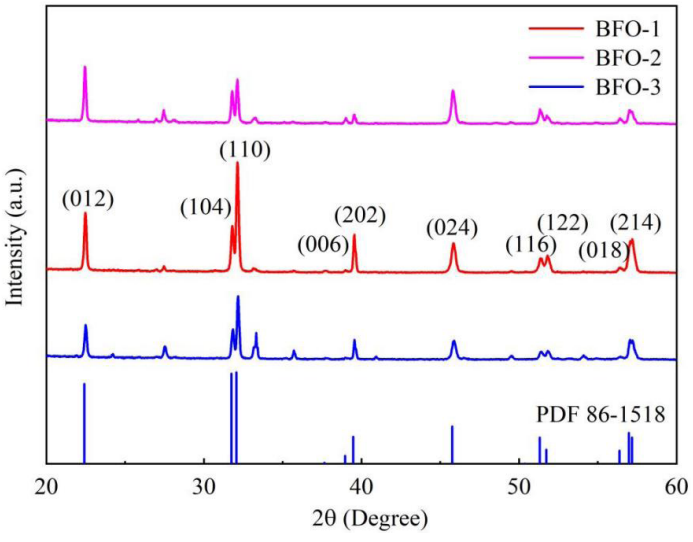

Figure 1. XRD diffraction pattern of pure-phase $BiFeO_3$ prepared under different conditions compared to the standard card: (a) BFO-1 (b) BFO-2 (c) BFO-3

3.2. SEM analysis

Figures 2(a) and **(b)** show the hydrothermally synthesized sample BFO-1, which exhibits an average diameter of approximately 50 μm when subjected to a reaction temperature of 180°C. The surface morphology consists of uniformly distributed spherical particles clustered together, revealing lamellar accumulation as depicted in **Figures 2(c)** and **(d)**. This observation is consistent with previous reports in the literature [13–14].

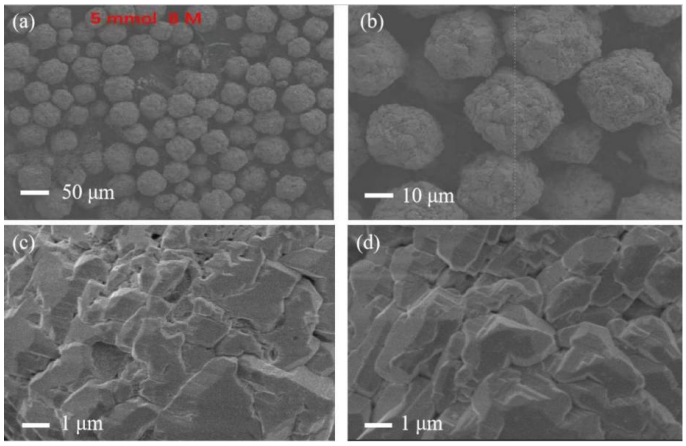

Figure 2. SEM image of BFO-1

3.3. XPS analysis

The XPS spectra in Figure 3(a) reveal the electronic valence states of Bi, Fe, and O in sample BFO-1. In **Figure 3(b)**, two peaks of Bi4f at 163.88 eV and 158.58 eV correspond to $Bi4f_{5/2}$ and $Bi4f_{7/2}$, respectively. The spin-orbit splitting energy of Bi4f is calculated to be 5.30 eV, which is consistent with well-documented values in the literature for the Bi^{3+} valence state, typically around 5.3 eV, thereby providing strong evidence for the presence of Bi^{3+} in $BiFeO_3$ [15]. In **Figure 3(c)**, the electron binding energies of $Fe2p_{1/2}$ and $Fe2p_{3/2}$ are observed at 724.14 eV and 710.46 eV, respectively, with a satellite peak at 712.54 eV. The spin-orbit splitting energy of Fe2p is 13.68 eV, indicating the presence of Fe in the Fe^{3+} valence state [16].

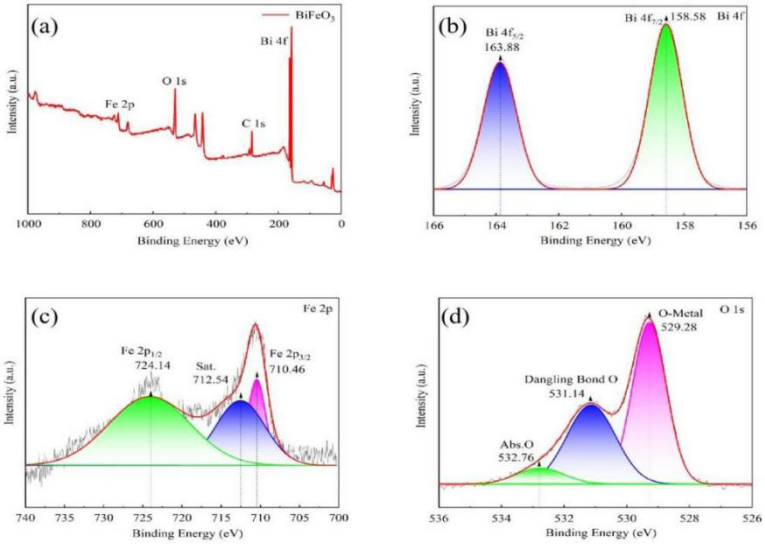

Figure 3. (a) XPS full spectrum of BFO-1 (b) Bi4f (c) Fe2p (d) O1s

Figure 3(d) shows three peaks in the O1s spectrum with electron binding energies at 532.76 eV, 531.14 eV, and 529.28 eV, corresponding to surface-adsorbed oxygen, lattice oxygen, and metal-oxygen bonds, respectively [17]. The presence of surface-adsorbed oxygen indicates the generation of oxygen vacancies, which favor the adsorption of tetracycline molecules. This not only reduces the electron-hole pair recombination rate but also facilitates the separation and transfer of photogenerated carriers, thereby enhancing photocatalytic and quantum efficiencies [18].

3.4. Evaluation of photocatalytic degradation performance of tetracycline

Figure 4(a) presents the absorption spectra of the tested tetracycline (TC) solutions, monitored using the UV-2450 spectrophotometer to assess photocatalytic degradation. Notably, the maximum absorbance corresponding to the 357 nm wavelength of the TC decreases during the photocatalytic process. Typically, tetracyclines exhibit strong absorption in the ultraviolet-visible (UV-Vis) range, particularly around 275–280 nm, which is associated with the benzene ring structure, and 350–360 nm, linked to the naphthalene ring and conjugated double bonds. During photocatalytic degradation, these absorption peaks diminish as tetracyclines are broken down into smaller, non-absorbing compounds. This decline indicates a steady reduction in tetracycline concentration, suggesting that active species such as hydroxyl radicals (•OH) and holes (h^+) played a crucial role in effectively degrading the tetracycline solution. The degradation rate was calculated to be approximately 27% after 120 minutes of photocatalysis, using **Equations 1** and **2** as shown in **Figure 4(b)**.

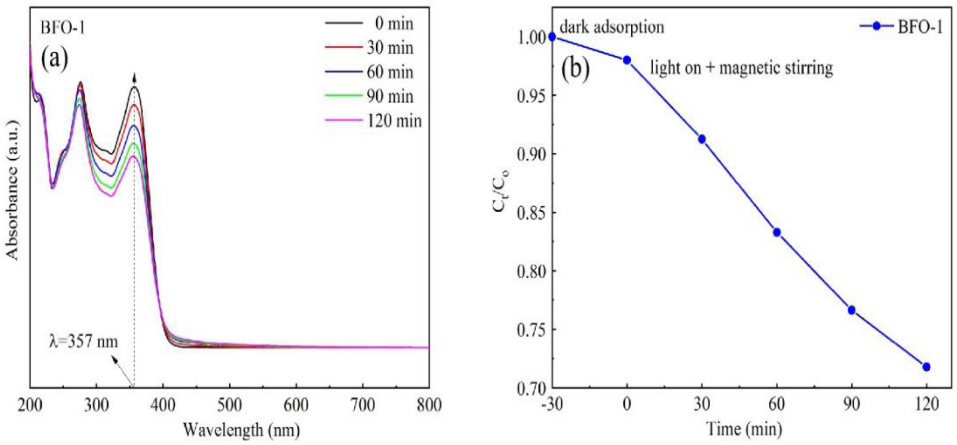

Figure 4. (a) BFO-1 degradation of tetracycline solution(b) BFO-1 degradation rate

3.5. Proposed mechanism of photocatalysis

Figure 5(a) shows the UV-VIS-DRS spectrum of the BFO-1 sample, which exhibits a broad absorption range within the visible wavelength spectrum, with the largest visible wave absorption edge at 530 nm. This expanded absorption spectrum suggests that BFO-1 can effectively absorb and respond to various wavelengths, indicating a robust photon absorption capability. This makes it more readily excited by light, resulting in the generation of a significant number of photogenerated electron-hole pairs, which could enhance its photocatalytic degradation efficiency [19–20]. The bandgap of the semiconductor material can be estimated using the equation $(\alpha h\nu)^n = A(h\nu - Eg)$, where α represents the absorption coefficient, h signifies Planck's constant, ν denotes the frequency of the absorbed photons, Eg refers to the bandgap value of the semiconductor, A is a constant, and n is a coefficient that

correlates with the semiconductor's characteristics (2 for direct bandgap semiconductors and 1/2 for indirect ones). Therefore, according to Figure 5(b), the bandgap value (Eg) of the BFO-1 sample is determined at about 2.34 eV.

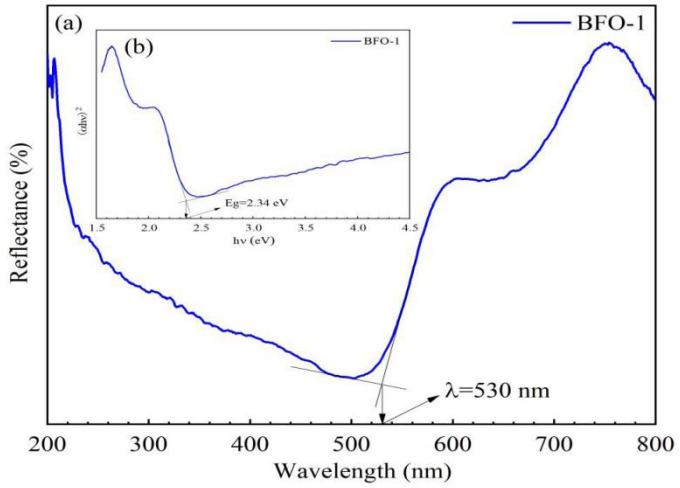

Figure 5. (a) UV-VIS-DRS plot of BFO-1 (b) Bandgap diagram of Tauc curve of BFO-1

X is the absolute electronegativity of $BiFeO_3$ semiconductors is about 5.89 eV, and Ee is the free electron energy of 4.5 eV on the atomic scale of H. According to Equations 3 and 4, E_{VB} = 2.56 eV, E_{CB} = 0.22 eV [21].

$$E_{VB} = X - Ee + 0.5Eg \quad (3)$$

$$E_{CB} = E_{VB} - Eg \quad (4)$$

$BiFeO_3 + hv \rightarrow e^- + h^+$

$e^- + O_2 \rightarrow \bullet O_2^-$

$h^+ + H_2O \rightarrow \bullet OH + H^+$

$h^+ + OH^- \rightarrow \bullet OH$

; $(h^+, \bullet OH) + TC$ CO_2, H_2O, inorganic compound

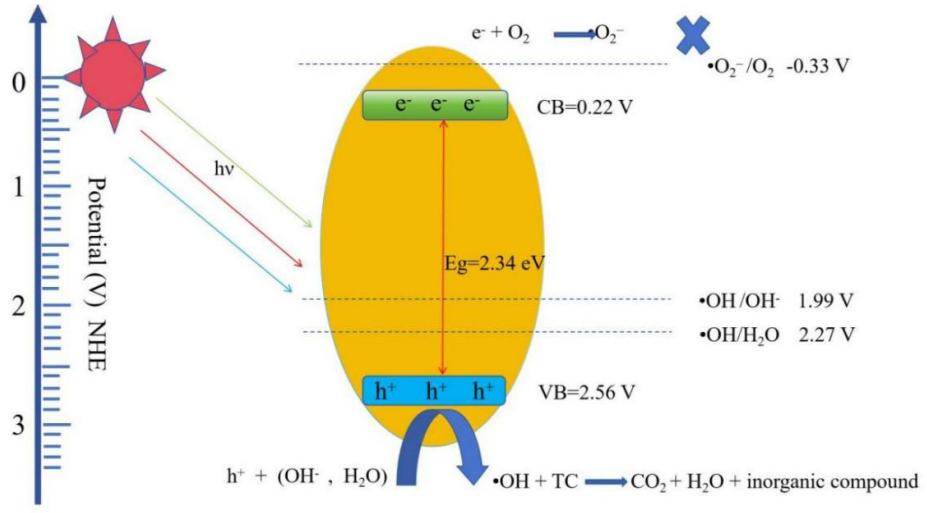

Figure 6. Energy band structure and photocatalytic mechanism of BFO-1

4. Conclusion

In this study, pure-phase $BiFeO_3$ was successfully synthesized using a simple hydrothermal method at 180°C. The synthesized material exhibited an agglomerated spherical morphology. The UV-VIS-DRS spectrum revealed that the energy bandgap of the synthesized BFO-1 was approximately 2.34 eV. Photocatalytic degradation experiments demonstrated that BFO-1 achieved a degradation efficiency of around 27% for tetracycline (TC) after 120 minutes, The primary active species responsible for TC degradation were •OH radicals, with h^+ playing a synergistic role.

Disclosure statement

The author declares no conflict of interest.

Reference

[1] Li Q, Zheng Y, Guo L, et al., 2024, Microbial Degradation of Tetracycline Antibiotics: Mechanisms and Environmental Implications. Journal of Agricultural and Food Chemistry, 72(24): 13523–13536.

[2] Xie Z, Tang J, Wu X, et al., 2019, Bioconcentration, Metabolism and the Effects of Tetracycline on Multiple Biomarkers in Chironomus Riparius Larvae. Science of The Total Environment, 2019(649): 1590–1598.

[3] Jeong J, Song W, Cooper WJ, et al., 2010, Degradation of Tetracycline Antibiotics: Mechanisms and Kinetic Studies for Advanced Oxidation/reduction Processes. Chemosphere, 78(5): 533–540.

[4] Wang J, Zhi D, Zhou H, et al., 2018, Evaluating Tetracycline Degradation Pathway and Intermediate Toxicity during the Electrochemical Oxidation over a Ti/Ti4O7 Anode. Water Research, 2018(37): 324–334.

[5] Tang X, Ni L, Han J, et al., 2017, Preparation and Characterization of Ternary Magnetic g-C3N4 Composite Photocatalysts for Removal of Tetracycline under Visible Light. Chinese Journal of Catalysis, 38(3): 447–457.

[6] Qu LL, Wang N, Li YY, et al., 2017, Novel Titanium Dioxide–Graphene–Activated Carbon Ternary Nanocomposites with Enhanced Photocatalytic Performance in Rhodamine B and Tetracycline Hydrochloride Degradation. Journal of Materials Science, 52(13): 8311–8320.

[7] Khan N, Sapi A, Arora I, et al., 2024, Photocatalytic CO2 Reduction using Metal and Nonmetal Doped TiO2 and its Mechanism. Reaction Kinetics, Mechanisms and Catalysis, 137(2): 629–655.

[8] Gao F, Chen XY, Yin KB, et al., 2007, Visible-Light Photocatalytic Properties of Weak Magnetic BiFeO3 Nanoparticles. Advanced Materials, 19(19): 2889–2892.

[9] Huo Y, Miao M, Zhang Y, et al., 2011, Aerosol-spraying Preparation of a Mesoporous Hollow Spherical BiFeO3 Visible Photocatalyst with Enhanced Activity and Durability. Chemical Communications, 47(7): 2089–2091.

[10] Zhu KM, Ma SY, Pei ST, et al., 2019, Preparation, Characterization and Formaldehyde Gas Sensing Properties of Walnut-shaped BiFeO3 Microspheres. Materials Letters, 2019(246): 107–110.

[11] Rajitha B, Rao KV, Suvarna R, 2020, Synthesis of Multiferroic BiFeO3 Microcrystals for Photocatalytic Activity and Stability Performance. Materials Today: Proceedings, 2020(26): 126–129.

[12] Wang N, Luo X, Han L, et al., 2020, Structure, Performance, and Application of BiFeO3 Nanomaterials. Nano-Micro Letters, 12(1): 81.

[13] Tong T, Cao W, Zhang H, et al., 2015, Controllable Phase Evolution of Bismuth Ferrite Oxides by an Organic Additive Modified Hydrothermal Method. Ceramics International, 2015(41): S106–S110.

[14] Tong T, Chen J, Jin D, et al., 2017, Preparation and Gas Sensing Characteristics of BiFeO3 Crystallites. Materials Letters, 2017(197): 160–162.

[15] Di L, Yang H, Xian T, et al., 2017, Enhanced Photocatalytic Activity of NaBH4 Reduced BiFeO3 Nanoparticles for Rhodamine B Decolorization. Materials, 10(10): 1118.

[16] Basith MA, Yesmin N, Hossain R, 2018, Low Temperature Synthesis of BiFeO3 Nanoparticles with Enhanced Magnetization and Promising Photocatalytic Performance in Dye Degradation and Hydrogen Evolution. RSC Advances, 8(52): 29613–29627.

[17] Chen D, Niu F, Qin L, et al., 2017, Defective BiFeO3 with Surface Oxygen Vacancies: Facile Synthesis and Mechanism Insight into Photocatalytic Performance. Solar Energy Materials and Solar Cells, 2017(171): 24–32.

[18] Hossain MS, Palanivel B, Rokhum SL, et al., 2023, Bismuth Ferrite (BiFeO3) 2D-nanoflakes for the Photocatalytic Degradation of Chromogenic Dyes under Solar Irradiation. Surfaces and Interfaces, 2023(41): 103240.

[19] Xue Z, Wang T, Chen B, et al., 2015, Degradation of Tetracycline with BiFeO3 Prepared by a Simple Hydrothermal Method. Materials, 8(9): 6360–6378.

[20] Li X, Jia F, Chen J, et al., 2023, Enhanced Photocatalytic Activity of Tourmaline Modified BiFeO3 Nanoparticles by Efficient Charge Transfer. Ceramics International, 49(21): 34147–34154.

[21] Mithun Prakash R, Ningaraju C, Gayathri K, et al., 2022, One-step Solution Auto-combustion Process for the Rapid Synthesis of Crystalline Phase Iron Oxide Nanoparticles with Improved Magnetic and Photocatalytic Properties. Advanced Powder Technology, 2022, 33(2): 103435.